IEEE TRANSACTIONS ON ELECTROMAGNETIC COMPATIBILITY, VOL. 64, NO. 1, FEBRUARY 2022

Prepreg and Core Dielectric Permittivity (ε_r) Extraction for Fabricated Striplines' Far-End Crosstalk Modeling

Shaohui Yong, *Member, IEEE*, Srinath Penugonda, *Student Member, IEEE*, DongHyun Kim, Victor Khilkevich, *Member, IEEE*, Bo Pu, *Member, IEEE*, Xiaoning Ye, Qian Gao, Xiao-Ding Cai, *Member, IEEE*, Bidyut Sen, and Jun Fan, *Fellow, IEEE*

***Abstract*—As the data rate and density of digital high-speed systems are getting higher, far-end crosstalk (FEXT) noise becomes one of the major issues that limit signal integrity performance. It was commonly believed that FEXT would be eliminated for striplines routed in a homogeneous dielectric, but in reality, FEXT can always be measured in striplines on the fabricated printed circuit boards. A slightly different dielectric permittivity (ε_r) of prepreg and core may be one of the major contributors to the FEXT. This article is focusing on providing a practical FEXT modeling methodology for striplines by introducing an approach to extract ε_r of prepreg and core. Using the known cross-sectional geometry and measured *S*-parameters of the coupled stripline, the capacitance components in prepreg and core are separated using a two-dimensional solver, and the ε_r of prepreg and core is determined. A more comprehensive FEXT modeling approach is proposed by applying extracted inhomogeneous dielectric material information.**

***Index Terms*—Dielectric material, far-end crosstalk (FEXT), stripline, transmission-line theory.**

I. Introduction

As DIGITAL systems are moving in the direction of faster data transmission rate and higher density of circuits, the problem of the far-end crosstalk (FEXT) becomes one of the major limiting factors for signal integrity performance [1]–[3].

The concept of FEXT due to inhomogeneous dielectric material was presented in [4]–[8] using microstrip line as the device under test (DUT), and the analytical crosstalk estimation formulas were derived by modal analysis. By modeling FEXT using the superposition of received even- and odd-mode signals on the victim line [8, Fig. 4]–[30], it was determined that the difference in phase velocities of even- and odd-mode signals caused by inhomogeneous dielectric material is the root cause of FEXT. Namely, if the odd and even components of the signal arrive at the receiver end at different times the 180° phase shift between them is no longer present and FEXT is generated.

The inhomogeneous dielectric material is almost unavoidable in fabricated multilayer printed circuit boards (PCB) due to the different glass fiber weave/contents in prepreg and core, prepreg melting during lamination, epoxy resin properties tolerances, etc. [9]–[12]. Engineers may measure noticeable FEXT on striplines and meet difficulties in FEXT modeling due to the unknown dielectric permittivity of prepreg and core.

Recently, several dielectric material properties extraction methods [13]–[16] and FEXT models [17]–[19] for fabricated striplines were proposed; however, all of them assumed a perfectly homogeneous dielectric material. In one of the models, a new concept called FEXT due to lossy conductors was proposed, which can be one of the major FEXT contributors in the high-speed striplines. As shown in [18], the proximity effect due to the lossy conductors causes different per-unit-length (PUL) resistances and, hence, attenuations for even and odd modes, leading to FEXT due to the superposition of the received evenand odd-mode signals with different rise times.

However, as far as the authors knowledge, there have been no published approaches for the characterization of the FEXT due to inhomogeneous dielectric material in striplines. As the examples, as shown in Section IV of the article, demonstrate, obvious discrepancies can be observed by comparing the measurement and modeled FEXT assuming homogeneous dielectric material.

In this article, to improve the FEXT modeling results, an approach is proposed to extract the relative permittivity ε_r of prepreg and core using the measured *S*-parameters and knowncross-sectionalgeometryofcoupledstriplines.Improved modeling results will be presented by comparing measurements with modeling results obtained using the extracted dielectric parameters.

ManuscriptreceivedNovember17,2020;revisedFebruary17,2021andApril 25, 2021; accepted May 19, 2021. Date of publication June 10, 2021; date of current version February 17, 2022. This work was supported in part by the NationalScienceFoundationunderGrantIIP-1440110.*(Correspondingauthor: Jun Fan.)*

Shaohui Yong, Srinath Penugonda, DongHyun Kim, Victor Khilkevich, Bo Pu, and Jun Fan are with the Electromagnetic Compatibility Laboratory, Missouri University of Science and Technology, Rolla, MO 65401 USA (e-mail: sy2m5@mst.edu; spr33@mst.edu; dkim@mst.edu; khilkevichv@mst.edu; bpdbh@mst.edu; jfan@mst.edu).

Xiaoning Ye is with Intel Corp., Hillsboro, OR 97124 USA (e-mail: xiaoning.ye@intel.com).

Qian Gao, Xiao-Ding Cai, and Bidyut Sen are with the Cisco Systems, Inc., San Jose, CA 95134 USA (e-mail: annagao@cisco.com; kecai@cisco.com; bisen@cisco.com).

Color versions of one or more figures in this article are available at https://doi.org/10.1109/TEMC.2021.3083771.

Digital Object Identifier 10.1109/TEMC.2021.3083771

Therestofthisarticleisorganizedasfollows.InSectionII,the transmission-linetheoryand analytical expressions ofFEXT are shown, and the impact of inhomogeneous dielectric material on FEXT is presented using simulation. By analyzing the electric field of striplines, the simulation results are explained by a qualitativetheorydescribingthepolarityofFEXT.InSectionIII, the algorithm of the prepreg and core permittivity extraction is introduced. Section IV provides the validations by comparing the measurement data with the results of modeling using the extracted ε_r. Finally, Section V concludes this article.

II. FEXT on the Stripline With Inhomogeneous Dielectric Material

A. FEXT Modeling Based on Modal Analysis

Before describing the extraction method, we would like to define the necessary parameters. In this article, the idea of describingFEXTbasedonthemodalanalysisisadopted[8].For apairofcoupledstriplines,aftertheaggressorsignalisseparated into even and odd modes, the FEXT is generated during the time interval between the arrival of the odd-mode signal and the arrival of the even-mode signal. In other words, after the propagation of l meters, the FEXT is the superposition of the received even- and odd-mode signals ($v_{\text{even}}(t,l)$, $v_{\text{odd}}(t,l)$) on the victim line [8, Fig. 4]–[30].

$$v_{\text{fext}}(t,l) = v_{\text{even}}(t,l) + v_{\text{odd}}(t,l). \tag{1}$$

Suppose that only the FEXT due to inhomogeneous dielectric exists (all other FEXT sources are neglected). Under the lossless transmission-line assumption, (1) can be expressed using a function of modal phase velocities to predict the peak value of FEXT [18, eq. (3)]

$$v_{\text{fext}} = \frac{1}{2}\cdot\frac{l}{t_r}\cdot\left(\frac{1}{v_{p,\text{odd}}} - \frac{1}{v_{p,\text{even}}}\right)\cdot v_I \tag{2}$$

where v_I is the amplitude of the aggressor signal that has a rise time of t_r. The odd and even phase velocities ($v_{p,\text{odd}}$, $v_{p,\text{even}}$) can be expressed using the PUL modal inductance (L_m) and capacitance (C_m)

$$v_{p,m} = \frac{1}{\sqrt{L_m C_m}}. \tag{3}$$

Here, m represents the even or odd mode. L_m and C_m can be obtained by the modal transformation of the nodal inductance (L) and capacitance (C) matrices of a three-conductor model with symmetrical signal traces [20], [21]

$$(\mathsf{T}_v)^{-1}\cdot \mathsf{L}\cdot \mathsf{T}_i = \begin{bmatrix} L_{11}+L_{21} & 0 \\ 0 & L_{11}-L_{21} \end{bmatrix} = \begin{bmatrix} L_{\text{even}} & 0 \\ 0 & L_{\text{odd}} \end{bmatrix} \tag{4}$$

$$(\mathsf{T}_i)^{-1}\cdot \mathsf{C}\cdot \mathsf{T}_v = \begin{bmatrix} C_{11}-|C_{21}| & 0 \\ 0 & C_{11}+|C_{21}| \end{bmatrix} = \begin{bmatrix} C_{\text{even}} & 0 \\ 0 & C_{\text{odd}} \end{bmatrix} \tag{5}$$

where

$$\mathsf{L} = \begin{bmatrix} L_{11} & L_{21} \\ L_{21} & L_{11} \end{bmatrix} \text{ and } \mathsf{C} = \begin{bmatrix} C_{11} & -|C_{21}| \\ -|C_{21}| & C_{11} \end{bmatrix} \tag{6}$$

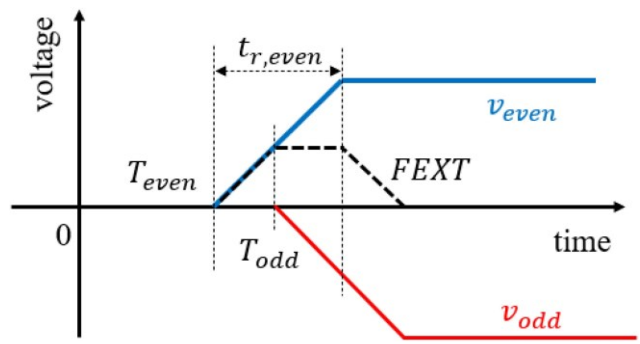

Fig. 1. Illustration of FEXT when $v_{p,\text{even}} > v_{p,\text{odd}}$. v_{even} and v_{odd} stand for the even- and odd-mode signals at the receiver end, respectively.

$$\mathsf{T}_v = \boldsymbol{T_i} = \begin{bmatrix} \frac{1}{\sqrt{2}} & \frac{-1}{\sqrt{2}} \\ \frac{1}{\sqrt{2}} & \frac{1}{\sqrt{2}} \end{bmatrix}. \tag{7}$$

For the homogeneous and lossless case, the FEXT is zero due to the same phase velocity for even- and odd-mode signals ($v_{p,\text{odd}} = v_{p,\text{even}}$), which can be proven by using an important identity for homogeneous media $\mathsf{LC} = \mathsf{CL} = \mu\varepsilon \mathsf{I}_n$ [20, eq. (3.37)].

The polarity of FEXT peak voltage can be explained by the modal analysis. First, for striplines with an inhomogeneous dielectric material and different thicknesses of dielectric layers, the modal velocities are not equal ($v_{p,\text{odd}} \neq v_{p,\text{even}}$). As Fig. 1 illustrates, for the positive aggressor signal, if the even-mode signal has a faster phase velocity and arrives at the receiver end earlier, the FEXT peak is positive. On the contrary, if the odd-mode signal propagates faster, the FEXT peak is negative.

B. Impact of the Inhomogeneous Dielectric on the Total FEXT of Striplines

Thevelocities$v_{p,\text{odd}}$ and$v_{p,\text{even}}$ ofapairofcoupledstriplines are determined by the cross-sectional geometry and material parameters; therefore, the prepreg and core dielectric permittivity ($\varepsilon_{r,pg}$, $\varepsilon_{r,co}$) plays an important role. To demonstrate FEXTs sensitivity to the prepreg and core inhomogeneity, several simulations are performed using an Ansys two-dimensional (2-D) extractor[22].Weusethecoupledstriplineswithcross-sectional geometry, as illustrated in Fig. 2. The thickness of prepreg is larger than the thickness of the core (h_{pg} = 12 mil > h_{co} = 8mil). The line length is 10 in, and the rise time of the aggressor signal is t_r = 35 ps. The dissipation factor ($\tan\delta$) in prepreg and core is equal to 0.003. All ports are matched.

As Table I presents, the dielectric constant in core ($\varepsilon_{r,co}$) is set to 3.4, and the dielectric constant in prepreg ($\varepsilon_{r,pg}$) is swept from 3.5 to 3.3 to investigate the impact of dielectric material inhomogeneity. The variation is approximately 10%, which is very likely to be expected for fabricated striplines [9].

The simulation results are given in Table I and Fig. 3. We observe that the impact from FEXT due to inhomogeneous dielectric material is noticeable. For this case with prepreg thickerthancore(h_{pg} = 12mil > h_{co} = 8mil),whenfor$\varepsilon_{r,pg} > \varepsilon_{r,co}$, the FEXT "bump" is increased by the inhomogeneous

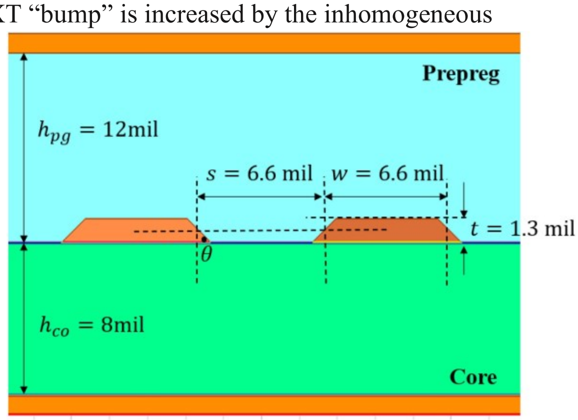

Fig. 2. Cross-sectional geometry of two coupled symmetrical stripline traces. The upper blue block represents the prepreg, and the lower green block stands for the core. The etching angle θ is 45°.

TABLE I
SIMULATION RESULTS OF THE STRIPLINES WITH COPPER TRACES AND REFERENCE PLANES

	#1	#2	#3	#4	#5
$\varepsilon_{r,pg}$	3.5	3.45	3.4	3.35	3.3
$\varepsilon_{r,co}$	3.3	3.35	3.4	3.45	3.5
FEXT peak value [mV]	33.3	19.9	7.3	-7.8	-21.5

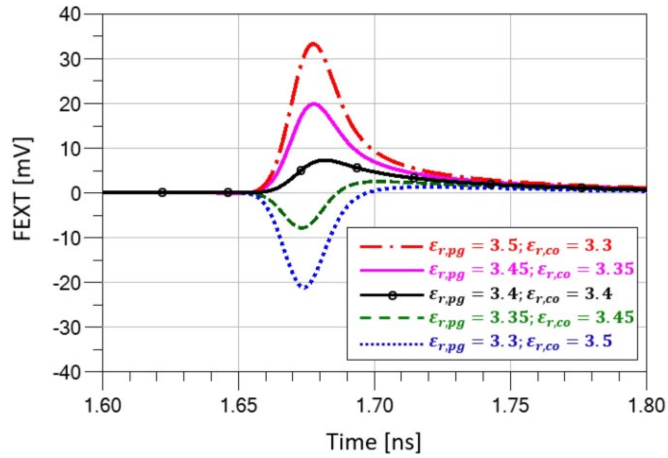

Fig. 3. Comparison between the cases with swept $\varepsilon_{r,pg}$ and $\varepsilon_{r,co}$. The striplinesundertestarewithcoppertracesandreferenceplanes(theconductivity equals 5.8e[7] S/m).

dielectric. When $\varepsilon_{r,pg} < \varepsilon_{r,co}$, the "dip" is introduced. As the difference between $\varepsilon_{r,pg}$ and $\varepsilon_{r,co}$ increases, the "bump" and the "dip" grow significantly.

The simulation data show the necessity of obtaining $\varepsilon_{r,pg}$ and $\varepsilon_{r,co}$ to achieve accurate FEXT modeling for coupled striplines. The assumption of the homogeneous dielectric can even lead to the modeled FEXT with the wrong polarity (the $\varepsilon_{r,pg}$ and $\varepsilon_{r,co}$ extraction approach will be presented in Section III). In Section II-C, a qualitative theory is brought up to explain the simulation results that engineers can use to roughly predict the polarity

TABLE II
SIMULATION RESULTS OF THE STRIPLINES WITH PEC TRACES AND REFERENCE PLANES

	*1	*2	*3	*4	*5
$\varepsilon_{r,pg}$	3.5	3.45	3.4	3.35	3.3
$\varepsilon_{r,co}$	3.3	3.35	3.4	3.45	3.5
FEXT peak value [mV]	36.5	17.7	0	-18.5	-36.3

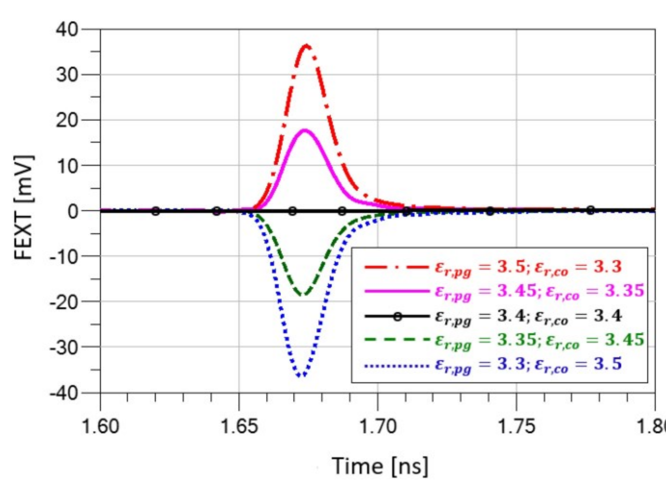

Fig. 4. Comparison between the cases with swept $\varepsilon_{r,pg}$ and $\varepsilon_{r,co}$. The striplines under test are with PEC traces and reference planes.

of FEXT using the information of dielectric material thickness (h_{pg}, h_{co}) and permittivity ($\varepsilon_{r,pg}$, $\varepsilon_{r,co}$).

C. Polarity of FEXT Due to Inhomogeneous Dielectric

According to the article presented in [18], when the dielectric material is homogeneous (case#3 in Fig. 3 and Table II, with $\varepsilon_{r,pg} = \varepsilon_{r,co}$), the FEXT with positive polarity can be explained because of FEXT due to lossy conductors. However, the relationship between the permittivity of prepreg and core and the polarity of FEXT needs further investigation.

To straightforward demonstrate FEXT due to inhomogeneous dielectric, another set of simulations is performed. The impact of FEXT due to lossy conductors is totally excluded by introducing perfect electric conductors (PEC). Compared with the simulation, as shown in Section II-B, all the settings are the same except that the traces and reference planes are modeled as PEC. The results are given in Fig. 4 and Table II.

For the homogeneous dielectric case (∗3), FEXT is equal to zero since FEXT due to lossy conductors is excluded. For the inhomogeneous cases (∗1, ∗2, ∗4, and ∗5), the noticeable "dip" and "bump" are exclusive due to dielectric inhomogeneity.

To provide explanations to the simulation results, first let us take a look at the expression of FEXT due to inhomogeneous dielectric, as shown in (2). To describe the differences between $v_{p,\text{even}}$ and $v_{p,\text{odd}}$, a variable Δ_{LC} is defined as

$$\Delta_{LC} = L_{\text{odd}} C_{\text{odd}} - L_{\text{even}} C_{\text{even}} = 2\left(L_{11}\left|C_{21}\right| - C_{11}L_{21}\right). \tag{8}$$

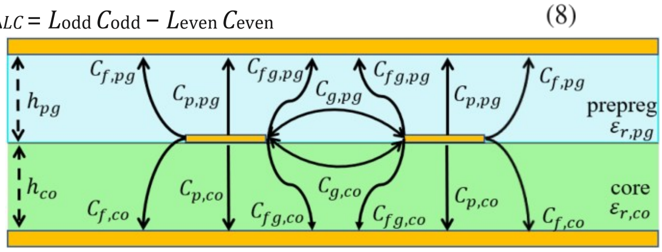

Fig. 5. Illustration of the capacitance components for the coupled striplines [23]. The prepreg and core dielectric heights are h_{pg} and h_{co}. The dielectric constant in prepreg and core is $\varepsilon_{r,pg}$ and $\varepsilon_{r,co}$.

The sign of Δ_{LC} determines the polarity of FEXT according to (2) and (3). Indeed, they are as follows.

1) If $\Delta_{LC} > 0$: $v_{p,\text{odd}} < v_{p,\text{even}}$ and FEXT is positive.
2) If $\Delta_{LC} < 0$: $v_{p,\text{odd}} > v_{p,\text{even}}$ and FEXT is negative.

To determine the influence of prepreg and core on Δ_{LC}, we use the idea, as presented in [23], and analyze the capacitance components. According to Fig. 5 [23, Fig. 2], there are four categories of the PUL capacitances in striplines as follows.

1) C_f: fringe capacitance on the outer side of the trace, contributed by the prepreg ($C_{f,pg}$) and core ($C_{f,co}$) regions.
2) C_p: parallel plate capacitance of the trace, contributed by the prepreg ($C_{p,pg}$) and core ($C_{p,co}$) regions.
3) C_{fg}: fringe capacitance near the gap between traces, contributed by the prepreg ($C_{fg,pg}$) and core ($C_{fg,co}$) regions.
4) C_g: mutual capacitance across the gap, contributed by the prepreg ($C_{g,pg}$) and core ($C_{g,co}$) regions.

The total capacitance in the prepreg ($C_{t,pg}$) is expressed using the capacitance components with subscript *pg*

$$\begin{aligned} C_{t,pg} &= C_{f,pg} + C_{p,pg} + C_{fg,pg} + C_{g,pg} = \varepsilon_{r,pg} \cdot \left(C^a_{f,pg} + C^a_{p,pg} + C^a_{fg,pg} + C^a_{g,pg}\right) \\ &= \varepsilon_{r,pg} \cdot \left(C^a_{\text{self},pg} + C^a_{g,pg}\right) = \varepsilon_{r,pg} \cdot C^a_{t,pg} \end{aligned} \tag{9a}$$

where

$$C^a_{\text{self},pg} = C^a_{f,pg} + C^a_{p,pg} + C^a_{fg,pg}.$$

This capacitance can be estimated using the scaling of the capacitances in the air-filled line (denoted by the superscript *a*) by the permittivity of the dielectric media [23]. Similarly, the total capacitance in the core ($C_{t,co}$) is expressed as

$$\begin{aligned} C_{t,co} &= C_{f,co} + C_{p,co} + C_{fg,co} + C_{g,co} = \varepsilon_{r,co} \cdot \left(C^a_{f,co} + C^a_{p,co} + C^a_{fg,co} + C^a_{g,co}\right) \\ &= \varepsilon_{r,co} \cdot \left(C^a_{\text{self},co} + C^a_{g,co}\right) = \varepsilon_{r,co} \cdot C^a_{t,co} \end{aligned} \tag{9b}$$

where $C^a_{\text{self},co} = C^a_{f,co} + C^a_{p,co} + C^a_{fg,co}$.

Thus, theself-capacitance inthe nodal capacitance matrixcan be expressed as

$$\begin{aligned} C_{11} &= C_{t,pg} + C_{t,co} = \varepsilon_{r,pg} \cdot \left(C^a_{\text{self},pg} + C^a_{g,pg}\right) \\ &\quad + \varepsilon_{r,co} \cdot \left(C^a_{\text{self},co} + C^a_{g,co}\right) \\ &= \varepsilon_{r,pg} \cdot C^a_{t,pg} + \varepsilon_{r,co} \cdot C^a_{t,co}. \end{aligned} \tag{10}$$

The mutual capacitance in the nodal capacitance matrix can be expressed as

$$\left|C_{21}\right| = C_{g,pg} + C_{g,co} = \varepsilon_{r,pg} \cdot C^a_{g,pg} + \varepsilon_{r,co} \cdot C^a_{g,co}. \tag{11}$$

According to the articles presented in [23, eq. (14)] and [24, eq. (14)], the self-inductance and mutual inductance can be estimated using the capacitances of the air-filled line as

$$L_{11}\,[\text{nH/cm}] \approx \frac{9\Delta C}{10C^a_{11}} = \frac{9\Delta C^a\left[(\text{pF/cm})^2\right]}{10\left(C^a_{t,pg} + C^a_{t,co}\right)[\text{pF/cm}]} \tag{12}$$

$$L_{21}\,[\mathrm{nH/cm}] \approx \frac{10\,|C_{21}^a|}{9\Delta C^a} = \frac{10\left(C_{g,pg}^a + C_{g,co}^a\right)[\mathrm{pF/cm}]}{9\Delta C^a\left[(\mathrm{pF/cm})^2\right]} \quad (13)$$

where $\Delta C^a = (C_{11}^a)^2 - (C_{21}^a)^2$. For typical edge-coupled striplines, $\Delta C^a > 0$. Next, let us calculate Δ_{LC} defined by (7) using the L and C given by (10)–(13)

$$\Delta_{LC} = \frac{10}{9\Delta C^a} \cdot (\varepsilon_{r,pg} - \varepsilon_{r,co}) \cdot \left(C_{t,pg}^a C_{g,co}^a - C_{t,co}^a C_{g,pg}^a\right). \quad (14)$$

According to the article presented in [25, eq. (6), Figs. 3 and 5], reducing dielectric layer thickness leads to an increase in total capacitance when the ratio of trace spacing to dielectric thickness is within the range from 0.02 to 1.5. Assuming this condition is true, we get

$$C_{t,pg}^a > C_{t,co}^a, \text{ when } h_{pg} < h_{co} \quad (15a)$$

$$C_{t,pg}^a < C_{t,co}^a, \text{ when } h_{pg} > h_{co}. \quad (15b)$$

In addition, according to the articles presented in [25, Fig. 4] and [26, eq. (5)], reducing dielectric thickness leads to a reduction in mutual capacitance when the ratio of trace spacing to dielectric thickness is within the range from 0.02 to 1.5; therefore

$$C_{g,pg}^a < C_{g,co}^a, \text{ when } h_{pg} < h_{co} \quad (16a)$$

$$C_{g,pg}^a > C_{g,co}^a, \text{ when } h_{pg} > h_{co}. \quad (16b)$$

According to (15) and (16), the third term in (14) subjects to the following conditions:

$$C_{t,pg}^a \cdot C_{g,co}^a - C_{g,pg}^a \cdot C_{t,co}^a > 0, \text{ when } h_{pg} < h_{co} \quad (17a)$$

$$C_{t,pg}^a \cdot C_{g,co}^a - C_{g,pg}^a \cdot C_{t,co}^a < 0, \text{ when } h_{pg} > h_{co}. \quad (17b)$$

Thus, by taking both (14) and (17) into account, the polarity of FEXT can be roughly estimated using the diagram, as shown in Fig. 6.

1) When the thicker dielectric layer has a lower permittivity, FEXT is negative.
2) When the thicker dielectric layer has a higher permittivity, FEXT is positive.

This rule of thumb has good correlation with the simulation data, as given in Tables I and II and Figs. 3 and 4. The FEXT due to the proximity of lossy conductor may lead to some estimation error when $\varepsilon_{r,pg}$ and $\varepsilon_{r,co}$ are close numerically (difference below 0.1), and the prediction is generally good when

The propagation constants are related to the PUL parameters of the modes as

$$\gamma_{\{cc,dd\}} = \sqrt{\left(R_{\{cc,dd\}} + j\omega L_{\{cc,dd\}}\right)\left(G_{\{cc,dd\}} + j\omega C_{\{cc,dd\}}\right)} \quad (20)$$

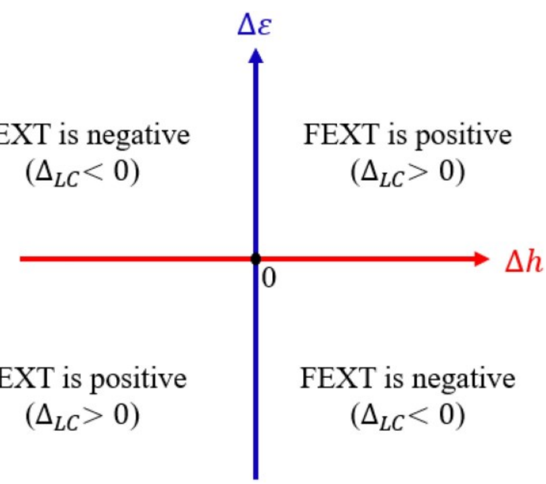

Fig. 6. Polarity of FEXT due to inhomogeneous dielectric can be estimated using dielectric height (h_{pg}, h_{co}) and permittivity ($\varepsilon_{r,pg}, \varepsilon_{r,co}$). Here, $\Delta h = h_{pg} - h_{co}$ and $\Delta\varepsilon = \varepsilon_{r,pg} - \varepsilon_{r,co}$.

the differences between h_{pg} and h_{co}, as well as $\varepsilon_{r,pg}$ and $\varepsilon_{r,co}$, are large enough.

III. Prepreg and Core Dielectric Permittivity Extraction Methodology

According to Section II, we can see that the stripline's FEXT is very sensitive to the differences between prepreg and core. The motivation of the part is to provide improved FEXT modeling results by taking inhomogeneous dielectric material into account.

A. Extraction Methodology

Using the qualitative theory in Fig. 6, engineers can estimate the polarity of FEXT on striplines using the cross-sectional geometry and nominal dielectric material information. However, as the simulation results in Table I and Figs. 3 and 4 demonstrate, FEXT is very sensitive to the difference in core and prepreg permittivities, and the nominal values of $\varepsilon_{r,pg}$ and $\varepsilon_{r,co}$ may not be known with enough precision to achieve the accuratemodelingofFEXTconsideringthatthePCBfabrication process may impact the dielectric properties. In this section, the authors will introduce the core and prepreg permittivity extraction methodology using the measured *S*-parameters and known cross-sectional geometry of a pair of coupled striplines.

For a pair of coupled striplines, suppose the propagation constants of the common and differential modes are known (measured)

$$\gamma_{\{cc,dd\}} = \alpha_{\{cc,dd\}} + j \cdot \beta_{\{cc,dd\}}. \tag{18}$$

Here, the real part of the propagation constant is the attenuation factor ($\alpha_{\{cc,dd\}}$), while the imaginary part is the phase constant ($\beta_{\{cc,dd\}}$). The phase constant can be obtained from the measured de-embedded transmission coefficient as

$$\beta_{\{cc,dd\}} = \left| \frac{\arg S_{\{cc,dd\}21}}{l} \right| \tag{19}$$

Sinceallpracticallinesarelowloss,thatis, $R \ll \omega L$ and $G \ll \omega C$,(20)canbeapproximatedusingtheTaylorseriesexpansion, and the phase constant can be estimated [27, eqs. (2–85b)] as

$$\beta_{\{cc,dd\}} \approx \omega \cdot \sqrt{L_{\{cc,dd\}} \cdot C_{\{cc,dd\}}}. \tag{21}$$

Thus, the modal capacitances can be obtained by using the measuredphaseconstant$\beta_{\{cc,dd\}}$ andthemodalPULinductance $L_{\{cc,dd\}}$ calculated using a 2-D solver for the air-filled line (this assumes that the inductance is not affected by the dielectric)

$$C_{cc} = \left(\frac{\beta_{cc}}{\omega}\right)^2 \cdot \frac{1}{L_{cc}} \tag{22a}$$

$$C_{dd} = \left(\frac{\beta_{dd}}{\omega}\right)^2 \cdot \frac{1}{L_{dd}}. \tag{22b}$$

According to the common and differential modal definition given in [20] and [21]

$$C_{cc} = 2 \cdot C_{\text{even}} = 2(C_{11} - |C_{21}|) \tag{23a}$$

$$C_{dd} = 0.5 \cdot C_{\text{odd}} = 0.5(C_{11} + |C_{21}|). \tag{23b}$$

By inserting (10) and (12) into (23), the relationship between $C_{cc,dd}$ and the permittivity of prepreg and core is expressed as

$$C_{cc} = 2\left(\varepsilon_{r,pg} \cdot C^a_{\text{self},pg} + \varepsilon_{r,co} \cdot C^a_{\text{self},co}\right) \tag{24a}$$

$$C_{dd} = 0.5\left[\varepsilon_{r,pg}\left(C^a_{\text{self},pg} + 2 \cdot \left|C^a_{g,pg}\right|\right) + \varepsilon_{r,co}\left(C^a_{\text{self},co} + 2 \cdot \left|C^a_{g,co}\right|\right)\right]. \tag{24b}$$

By solving the system of equations (24a) and (24b) , the permittivity of prepreg and core can be obtained as

$$\varepsilon_{r,co} = \frac{0.5 \cdot C_{cc} \cdot \left(C^a_{\text{self},pg} + 2 \cdot \left|C^a_{g,pg}\right|\right) - 2 \cdot C_{dd} \cdot C^a_{\text{self},pg}}{C^a_{\text{self},co}\left(C^a_{\text{self},pg} + 2\left|C^a_{g,pg}\right|\right) - C^a_{\text{self},pg}\left(C^a_{\text{self},co} + 2\left|C^a_{g,co}\right|\right)} \tag{25a}$$

$$\varepsilon_{r,pg} = \frac{0.5 \cdot C_{cc} \cdot \left(C^a_{\text{self},co} + 2 \cdot \left|C^a_{g,co}\right|\right) - 2 \cdot C_{dd} \cdot C^a_{\text{self},co}}{C^a_{\text{self},pg}\left(C^a_{\text{self},co} + 2\left|C^a_{g,co}\right|\right) - C^a_{\text{self},co}\left(C^a_{\text{self},pg} + 2\left|C^a_{g,pg}\right|\right)} \tag{25b}$$

Here, with the measured phase (19), the modal capacitances C_{cc} and C_{dd} can be obtained using (22). Thus, if the capacitance components $C^a_{g,pg}$, $C^a_{\text{self},pg}$, $C^a_{g,co}$, and $C^a_{\text{self},co}$ are calculated, the permittivity of prepreg and core will be available as (25) shows.Inaddition, (25)proves that $\varepsilon_{r,co}$ and $\varepsilon_{r,pg}$ aretheunique solutions of the known measured phase and cross-sectional geometry information.

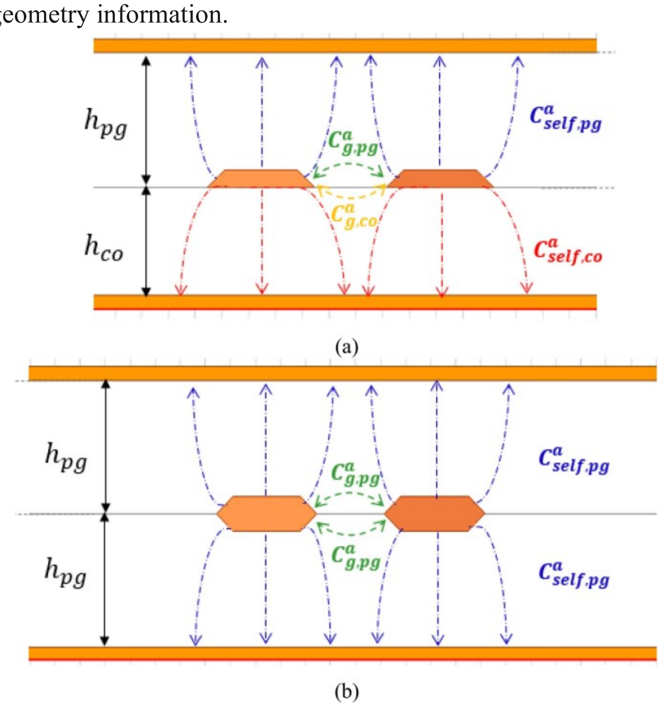

Fig.7. Twoadditional2-Dair-filledmodelswereproposedforthecapacitance calculation. (a) Model-A is repeating the actual geometry. (b) Model-B is a vertically mirrored prepreg layer.

In order to use (25) in practice, the capacitance components in core and prepreg regions need to be calculated. To achieve this, two additional 2-D models with air dielectric material are created using the known cross-sectional geometry. As Fig. 7(a) illustrates, the additional air-filled model-A is created using the exact geometry of the coupled striplines. The self and mutual capacitances (C_{11}^{A} ,$|C_{21}^{A}|$)ofthismodelarecalculatedbythe2-D solver. By setting $\varepsilon_{r,pg} = \varepsilon_{r,co} = 1$, (10) and (11) are modified to describe C_{11A} and $|C_{21A}|$

$$C_{11}^{\mathrm{A}} = C_{\mathrm{self},pg}^{a} + C_{\mathrm{self},co}^{a} + C_{g,pg}^{a} + C_{g,co}^{a} \tag{26}$$

$$\left|C_{21}^{\mathrm{A}}\right| = C_{g,pg}^{a} + C_{g,co}^{a}. \tag{27}$$

As Fig. 7(b) shows, the additional air-filled model-B is vertically balanced, with the geometry of prepreg flipped down to substitutethelowerportionoftheoriginaltransmissionline.The capacitances in the upper portion and lower portion are the same due to symmetry. On the other hand, since the top part of both models is identical, we can reasonably assume that the $C_{g,pg}{}^{a}$ is equal for both models as well. Thus, by replacing $C_{g,co}{}^{a}$ with $C_{g,pg}{}^{a}$ in (26) and (27), the capacitance components of model-B can be expressed as

$$C_{11}^{\mathrm{B}} = 2 \cdot C_{\mathrm{self},pg}^{a} + 2 \cdot C_{g,pg}^{a} \tag{28}$$

$$\left|C_{21}^{\mathrm{B}}\right| = 2 \cdot C_{g,pg}^{a}. \tag{29}$$

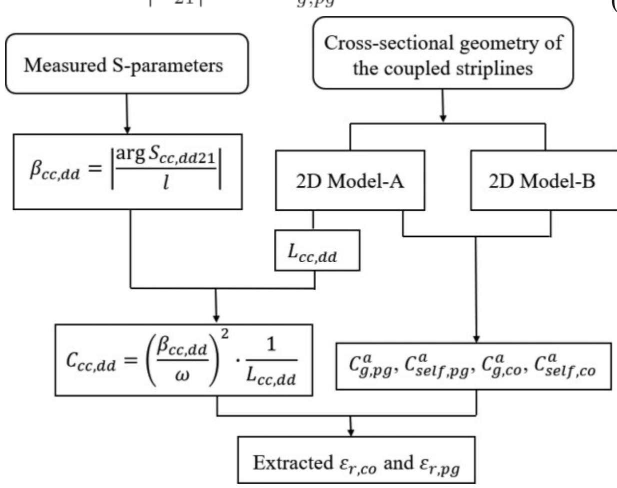

Fig. 8. Flowchart of the proposed $\varepsilon_{r,pg}$ and $\varepsilon_{r,co}$ extraction method.

By solving (26)–(29), the capacitance components needed for the permittivity extraction become available

$$C_{g,pg}^{a} = 0.5 \cdot \left|C_{21}^{\mathrm{B}}\right| \tag{30}$$

$$C_{\mathrm{self},pg}^{a} = 0.5 \cdot \left(C_{11}^{\mathrm{B}} - \left|C_{21}^{\mathrm{B}}\right|\right) \tag{31}$$

$$C_{g,co}^{a} = \left|C_{21}^{\mathrm{A}}\right| - 0.5 \cdot \left|C_{21}^{\mathrm{B}}\right| \tag{32}$$

$$C_{\mathrm{self},co}^{a} = C_{11}^{\mathrm{A}} - \left|C_{21}^{\mathrm{A}}\right| - 0.5 \cdot \left(C_{11}^{\mathrm{B}} - \left|C_{21}^{\mathrm{B}}\right|\right). \tag{33}$$

By inserting (22) and (30)–(33) into (25), the permittivity of prepregandcorecanbeextracted.Theflowchartoftheextraction is shown in Fig. 8.

B. Validation in Simulation

To illustrate the feasibility of the proposed method, it is first applied to a simulated transmission line. The accuracy of $\varepsilon_{r,pg}$ and $\varepsilon_{r,co}$ extraction is investigated.

A 2-D model of the coupled stripline with the cross-sectional dimensions, as indicated in Fig. 2, is created. Both core and prepreg are modeled according to the Djordjevic model [28] with the following parameters at 1 GHz: $\varepsilon_{r,pg} = 3.4$, $\tan\delta_{pg} = 0.012$, $\varepsilon_{r,co} = 3.6$, and $\tan\delta_{co} = 0.012$. The modal transmissioncoefficientsS_{cc21} andS_{dd21} arecalculatedbyusing Ansys 2-D extractor, and the obtained modal attenuation and phase constants (the latter is normalized by the frequency to reveal the nonlinear dependence of the phase on the frequency) are shown in Fig. 9.

The core and prepreg permittivity extraction is performed according to Fig. 8 and the comparisons between the actual and extracted $\varepsilon_{r,pg}$ and $\varepsilon_{r,co}$ are shown in Fig. 10. The relative error is below 2% for frequencies above 0.1 GHz. Even though the error goes up to about 10% at frequencies below 0.01 GHz due to reduced difference between β_{cc} and β_{dd} when the simulation accuracy becomes a major limiting factor, we would like to conclude that the proposed algorithm has acceptable accuracy for the bandwidth from at least 0.1 to 50 GHz.

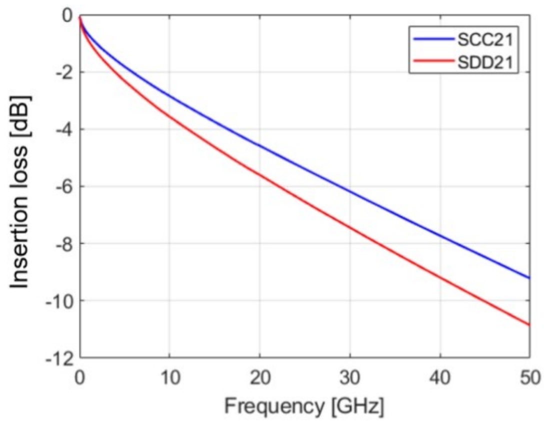

(a)

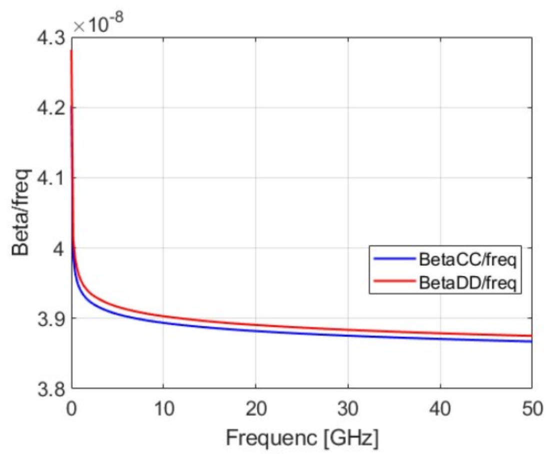

(b)

Fig. 9. (a) Simulated insertion loss and (b) phase of the coupled stripline. To present the frequency dependence of phase, $\beta_{\{cc,dd\}}/f$ is presented.

IV. Tests Based on Fabricated PCB

To test the proposed method, a validation board containing multiple lines was fabricated. The cables are connected to the PCB using the high-precision surface mount SMA(SubMiniatureversionA)connectors.Twoofthelines(1.3 in and 15.98 in) were used for 2x-thru measurements [29–33]. The S-parameters measurement is performed using a Keysight N5244A 4-port network analyzer. The VNA(Vector Network Analyzer) calibration is performed using an electronic calibration kit N4692 up to 50 GHz. The cross-sectional geometry of the coupled lines is presented in Fig. 11. The de-embedded attenuation and phase constants are given in Fig. 12.

Theextracted$\varepsilon_{r,pg}$ and$\varepsilon_{r,co}$ areshowninFig.13plottedusing solid curves. Since the extraction results are directly influenced by inaccuracies in the input parameters, slight variations can be observed in the extracted curves due to VNA measurement inaccuracies, de-embedding deficiencies [13], etc. To enforce the causality of extracted $\varepsilon_{r,pg}$ and $\varepsilon_{r,co}$, which would allow using the extraction results for the time-domain simulations, the Djordjevic model is used to fit the initially extracted $\varepsilon_{r,pg}$ and $\varepsilon_{r,co}$.

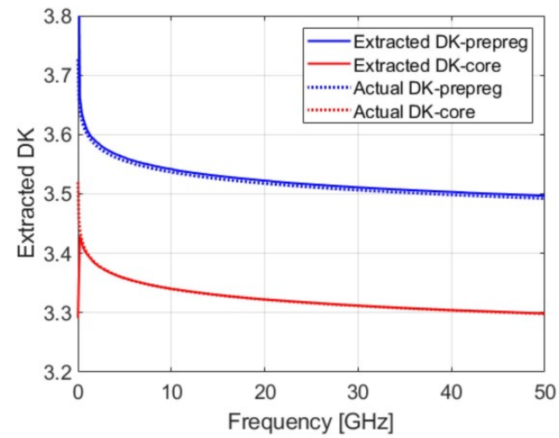

(a)

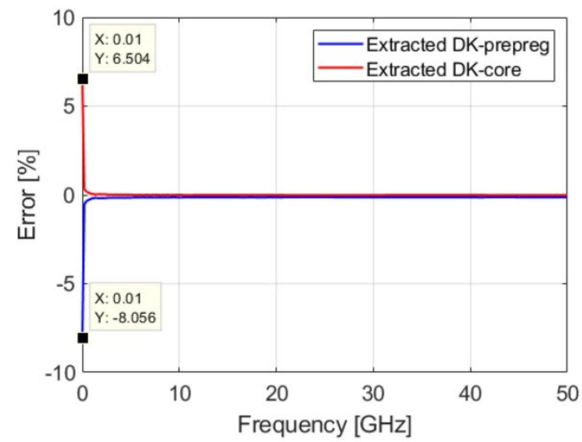

(b)

Fig. 10. (a) Comparison between the actual and extracted $\varepsilon_{r,pg}$ and $\varepsilon_{r,co}$. (b) Relative extraction error is also provided.

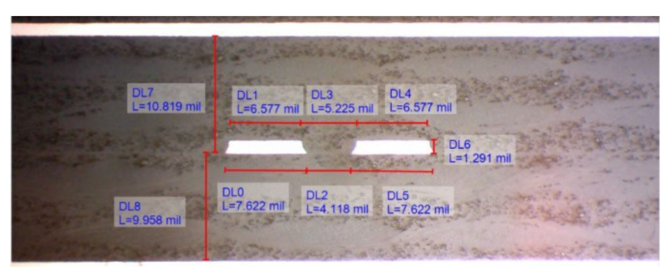

Fig. 11. Cross section of the coupled striplines.

Using the extracted tanδ (assuming equal values for core and prepreg) and conductor surface roughness parameters determined for the same line in [13], a model of the transmission line with the fitted core and prepreg parameters was created and used tocalculatetheFEXTsignalinthetimedomain.Thecomparison between the modeled and measured FEXT is shown in Fig. 14.

The incident signal on the aggressor line has the magnitude of 1 V and the rise time of 70 ps.

For reference, a model using the effective permittivity ($\varepsilon_{r,\mathrm{eff}}$ = 3.4@1 GHz) extracted assuming a homogeneous dielectric material [13] is also used for FEXT modeling (blue dashedcurveinFig.14).Thesurfaceroughnesswasmodeledusingt heHuraymodel.TheHuraymodelhadthefollowingparameters: ball size $a_{\mathrm{ball}} = 0.63\ \mu$m, number of balls $N_{\mathrm{ball}} = 25$, and the tile area $A_{\mathrm{tile}} = 90\ \mu\mathrm{m}^2$. The parameters for the roughness model were determined by an empirical approach, as presented in [34] and [35], using profiles, as shown in [13], with rms roughness of 0.43 μm. The extracted loss tangent ($\tan\delta$) is about 0.0025@1 GHz. A two-term Djordjevic model is used to describe the frequency dependence of the dielectric material properties [13]. By comparing the result of FEXT modeling using the homogeneous model to the measured signal, it becomes obvious that the homogeneous model fails to reproduce a dip at 1.6 ns. While by modeling FEXT using extracted $\varepsilon_{r,pg}$ and $\varepsilon_{r,co}$, the FEXT due to inhomogeneous dielectric material can be captured, and the dip at 1.6 ns is properly reproduced. The peak at 1.65 ns is explained by the FEXT due to the proximity effect of lossy conductor [18], and it is the major contributor to the total FEXT in this particular transmission line.

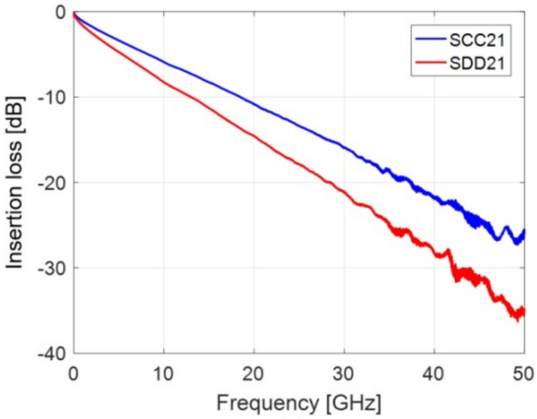

(a)

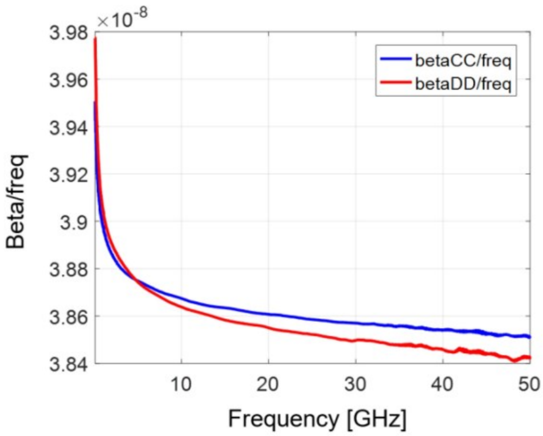

(b)

Fig. 12. (a) Measured insertion loss and (b) phase of the coupled stripline.

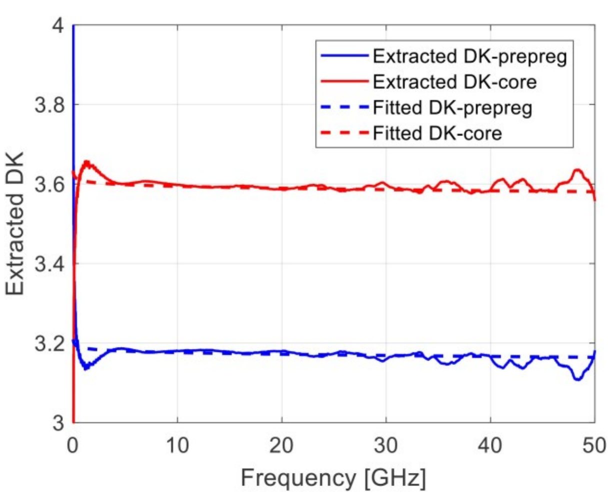

Fig. 13. Initially extracted (solid lines) and fitted (dotted lines) $\varepsilon_{r,pg}$ and $\varepsilon_{r,co}$. The values at 20 GHz are used to create the Djordjevic model.

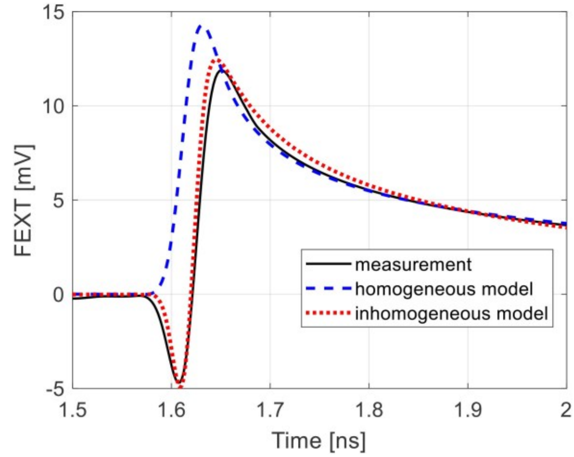

Fig. 14. Comparison of the time-domain FEXT between measurement (the solid line) and Q2D models created using extracted $\varepsilon_{r,pg}$ and $\varepsilon_{r,co}$ (dotted line). The modeling using extracted $\varepsilon_{r,\mathrm{eff}}$ assuming homogeneous dielectric material is also provided for the reference (the dashed line).

Notice that the authors did not present the FEXT sources' percentage contribution to the total FEXT because the "peak" or "valley" of different FEXT sources occurs at different times. FEXT due to inhomogeneous dielectric material is caused by different modal velocities, and the maximum amplitude occurs at the moment when the slower mode arrives, as shown in Fig. 1. FEXT due to lossy conductor is due to different rise times of the two modes, and the maximum amplitude occurs at the moment that the received even and odd waveforms are with their biggest differences. Thus, the maximum of the total FEXT waveform does not match the results of adding up the nonsimultaneous maximum amplitude of different FEXT sources.

At last, to achieve good extraction accuracy, we recommend to use the cross-sectional sample of the coupled striplines. Using the roughly estimated geometrical information to do the extraction will lead to lower accuracy unavoidably. A sensitivity test was performed previously, and we found that for the case undertest,theextractedpermittivity'ssensitivitytothedielectric thickness (h_{pg} and h_{co}) and trace thickness (t) is worth mentioning. Using the coupled striplines with geometry, as shown in Fig. 11, ±10% perturbation in h_{pg} and h_{co} and t will lead to 13%, 6%, and 3% change in extracted $\varepsilon_{r,pg}$.

TABLE III
FEXT CONTRIBUTORS FOR STRIPLINES

FEXT Contributors	Properties
Inhomogeneous dielectric material	Caused by the difference in modal components' propagation delay. The FEXT polarity is determined by geometry and inhomogeneous dielectric material.
Proximity of lossy conductors [18]	Caused by the difference in modal attenuation. The FEXT polarity is positive.
Mismatched terminals [19]	Caused by the reflection and backward coupling at the terminals.

V. CONCLUSION

It was demonstrated that FEXT is very sensitive to the inhomogeneous dielectric material of striplines. Even though the mechanism of FEXT due to inhomogeneous dielectric was revealed previously for microstrip lines, there has been no methodology to analyze the inhomogeneous dielectric material of the fabricated striplines. To estimate the polarity of FEXT due to inhomogeneous dielectric material, a rule of thumb is proposed using the geometry and material information of the coupled striplines.

Byanalyzingthecapacitancecomponentsinprepregandcore, a new dielectric permittivity extraction approach is proposed to characterize $\varepsilon_{r,pg}$ and $\varepsilon_{r,co}$. According to the tests based on the fabricatedPCB,usingtheextracted$\varepsilon_{r,pg}$ and$\varepsilon_{r,co}$,theimproved accuracy of FEXT modeling can be achieved compared with the modeling assuming homogeneous dielectric material.

Intheend,toprovidebetteroverviewofFEXTcontributorson striplines, Table III is provided. Using the techniques, as shown in [18] and [19] and this article, each FEXT contributor can be characterized.

REFERENCES

[1] B. Chen *et al.*, "Differential integrated crosstalk noise (ICN) reduction among multiple differential BGA and via pairs by using design of experiments (DoE) method," in *Proc. IEEE Int. Symp. Electromagn. Compat. Signal/Power Integrity*, Washington, DC, USA, 2017, pp. 112–117.

[2] B. Chen, S. Pan, J. Wang, S. Yong, M. Ouyang, and J. Fan, "Differential crosstalk mitigation in the pin field area of Serdes channel with trace routing guidance," *IEEE Trans. Electromagn. Compat.*, vol. 61, no. 4, pp. 1385–1394, Aug. 2019.

[3] B. Chen *et al.*, "Differential integrated crosstalk noise (ICN) mitigation in the pin field area of SerDes channel," in *Proc. IEEE Symp. Eectromagn. Compat., Signal Integrity Power Integrity*, Long Beach, CA, USA, 2018, pp. 533–537.

[4] E. Bracken, "Improved formulas for crosstalk coefficients," in *Proc. DesignCon*, 2016.

[5] C. R. Paul, "Literal solutions for time-domain crosstalk on lossless transmission lines," *IEEE Trans. Electromagn. Compat.*, vol. 34, no. 4, pp. 433–444, Nov. 1992.

[6] D.B.Jarvis,"Theeffectsofinterconnectionsonhigh-speedlogiccircuits," *IEEETrans.Electron.Comput.*,vol.EC-12,no.5,pp. 476–487,Oct.1963.

[7] W. Jiang, X.-D. Cai, B. Sen, and G. Wang, "Equation-based solutions to coupled, asymmetrical, lossy, and nonuniform microstrip lines for tabrouting applications," *IEEE Trans. Electromagn. Compat.*, vol. 61, no. 2, pp. 548–557, Apr. 2019.

[8] S. H. Hall and H. L. Heck, *Advanced Signal Integrity for High-Speed Digital Designs*. Hoboken, NJ, USA: Wiley, 2009.

[9] G. Brist, "Design optimization of single-ended and differential impedance PCB transmission lines," Intel Corp., Santa Clara, CA, USA. Accessed on: Apr. 2019. [Online]. Available: https://www.jlab.org/eng/eecad/pdf/053designop.pdf

[10] X. Tian *et al.*, "Numerical investigation of glass-weave effects on high-speed interconnects in printed circuit board," in *Proc. IEEE Int. Symp. Electromagn. Compat.*, Raleigh, NC, USA, 2014, pp. 475–479.

[11] D. Nozadze, A. Koul, K. Nalla, M. Sapozhnikov, and V. Khilkevich, "Effect of time delay skew on differential insertion loss in weak and strong coupled PCB traces," in *Proc. IEEE 26th Conf. Elect. Performance Electron. Packag. Syst.*, San Jose, CA, USA, 2017, pp. 1–3.

[12] J.He,S.Yong,Z.Kiguradze,A.Chada,B.Mutnury,andJ.Drewniak,"The effect of the parallel-plate mode on striplines in inhomogeneous dielectric media," in *Proc. IEEE Int. Symp. Electromagn. Compat. Signal/Power Integrity,* Reno, NV, USA, 2020, pp. 352–356.

[13] S. Yong *et al.*, "Dielectric loss tangent extraction using modal measurements and 2-D cross-sectional analysis for multilayer PCBs," *IEEE Trans. Electromagn. Compat.*, vol. 62, no. 4, pp. 1278–1292, Aug. 2020.

[14] S. Yong *et al.*, "Dielectric dissipation factor (DF) extraction based on differential measurements and 2-D cross-sectional analysis," in *Proc. IEEE Symp. Electromagn. Compat., Signal Integrity Power Integrity*, Long Beach, CA, USA, 2018, pp. 217–222, doi: 10.1109/EMCSI.2018.8495386.

[15] S. Jin, B. Chen, X. Fang, H. Gao, X. Ye, and J. Fan, "Improved 'rootomega' method for transmission-line-based material property extraction for multilayer PCBs," *IEEE Trans. Electromagn. Compat.*, vol. 59, no. 4, pp. 1356–1367, Aug. 2017.

[16] S. Yong *et al.*, "Dielectric material and foil surface roughness properties extraction based on single-ended measurements and phase constant (β) fitting," in *Proc. IEEE Int. Symp. Electromagn. Compat. Signal/Power Integrity*, Reno, NV, USA, 2020, pp. 346–351.

[17] K. Scharff, H.-D. Brüns, and C. Schuster, "Efficient crosstalk analysis of differential links on printed circuit boards up to 100 GHz," *IEEE Trans. Electromagn. Compat.*, vol. 61, no. 6, pp. 1849–1859, Dec. 2019.

[18] S.Yong,V.Khilkevich,X.-D.Cai,C.Sui,B.Sen,andJ.Fan,"Comprehensive and practical way to look at far-end crosstalk for transmission lines with lossy conductor and dielectric," *IEEE Trans. Electromagn. Compat.*, vol. 62, no. 2, pp. 510–520, Apr. 2020.

[19] S. Yong, K. Cai, B. Sen, J. Fan, V. Khilkevich, and C. Sui, "A comprehensive and practical way to look at crosstalk for transmission lines with mismatched terminals," in *Proc. IEEE Int. Symp. Electromagn. Compat., Signal Integrity Power Integrity*, Long Beach, CA, USA, 2018, pp. 538–543.

[20] C. R. Paul, *Analysis of Multiconductor Transmission Lines*, 2nd ed. New York, NY, USA: Wiley, 2008.

[21] T. Granberg, *Handbook of Digital Techniques for High Speed Design*. Hoboken, NJ, USA: Prentice Hall, 2004.

[22] "ANSYS electronics desktop online help–2D extractor," ANSYS, Inc., Canonsburg, PA, USA, 2019.

[23] S. S. Bedair, "Characteristics of some asymmetrical coupled transmission lines," *IEEE Trans. Microw. Theory Techn.*, vol. 32, no. 1, pp. 108–110, Jan. 1984.

[24] S. S. Bedair and I. Wolff, "Fast and accurate analytic formulas for calculating the parameters of a general broadside-coupled coplanar waveguide for (M)MIC applications," *IEEE Trans. Microw. Theory Techn.*, vol. 37, no. 5, pp. 843–850, May 1989.

[25] W. J. Getsinger, "Coupled rectangular bars between parallel plates," *IRE Trans. Microw. Theory Techn.*, vol. 10, no. 1, pp. 65–72, Jan. 1962.

[26] S. M. Perlow, "Analysis of edge-coupled shielded strip and slabline structures," *IEEE Trans. Microw. Theory Techn.*, vol. 35, no. 5, pp. 522–529, May 1987

[27] D.M.Pozar,*MicrowaveEngineering*,4thed.NewYork,NY,USA:Wiley, 2012.

[28] A. R. Djordjevic, R. M. Biljic, V. D. Likar-Smiljanic, and T. K. Sarkar, "Wideband frequency-domain characterization of FR-4 and time-domain causality,"*IEEETrans.Electromagn.Compat.,*vol.43,no.4,pp. 662–667, Nov. 2001.

[29] Q. Huang, J. Li, 1. Zhou, W. Wu, Y. Qi, and J. Fan, "De-embedding method to accurately measure high-frequency impedance of an O-shape spring contact," in *Proc. IEEE Int. Symp. Electromagn. Campat.*, 2014, pp. 600–603.

[30] Y. Liu *et al.*, "S-parameter de-embedding error estimation based on the statistical circuit models of fixtures," *IEEE Trans. Electromagn. Compat.*, vol. 62, no. 4, pp. 1459–1467, Aug. 2020.

[31] S. Yong *et al.*, "A practical de-embedding error analysis method based on statistical circuit models of fixtures," in *Proc. IEEE Int. Symp. Electromagn. Compat., Signal Power Integrity*, New Orleans, LA, USA, 2019, pp. 45–50.

[32] B. Chen, J. He, Y. Guo, S. Pan, X. Ye, and J. Fan, "Multi-ports (2^n) 2x-thru de-embedding: Theory, validation, and mode conversion characterization," *IEEE Trans. Electramagn. Compat.*, vol. 61, no. 4, pp. 1261–1270, Aug. 2019.

[33] B. Chen, X. Ye, B. Samaras, and J. Fan, "A novel de-embedding method suitable for transmission-line measurement," in *Proc. Asia-Pac. Symp. Electromagn. Compat.*, Taipei, Taiwan, 2015, pp. 1–4.

[34] S. Yong *et al.*, "A cross-sectional profile based model for stripline conductor surface roughness," in *Proc. IEEE Int. Symp. Electromagn. Compat. Signal/Power Integrity*, Reno, NV, USA, 2020, pp. 334–339.

[35] S. Yong *et al.*, "Resistance modeling for striplines with different surface roughness on the planes," in *Proc. IEEE Int. Symp. Electromagn. Compat. Signal/Power Integrity,* 2020, pp. 340–345.

ShaohuiYong(Member,IEEE)receivedtheM.S.andPh.D.degreesinelectrical engineering from the Missouri University of Science and Technology, Rolla, MO, USA, in 2015 and 2020, respectively.

He is currently a Staff Engineer with Marvell Technology, Inc., Santa Clara, CA, USA, responsible for electromagnetic interference and signal and power integrity of high-speed integrated circuit (IC) packaging. His research interests are in the areas of IC packaging, electromagnetic measurement and simulation techniques, and high-speed digital systems.

Srinath Penugonda (Student Member, IEEE) is currently working toward the Ph.D.degreewiththeDepartmentofElectricalEngineering,MissouriUniversity of Science and Technology, Rolla, MO, USA.

He joined Electromagnetic Compatibility Laboratory, Missouri University of Science and Technology, as a Graduate Research Assistant, in May 2014, and since then, he has been involved in various research projects. His main research interests include signal integrity and electromagnetics.

DongHyun Kim received the B.S., M.S., and Ph.D. degrees in electrical engineering from the Korea Advanced Institute of Science and Technology, Daejeon, South Korea, in 2012, 2014, and 2018, respectively.

In 2018, he joined the Missouri University of Science and Technology (formerly University of Missouri-Rolla), Rolla, MO, USA, where he is currently an Assistant Professor with Electromagnetic Compatibility (EMC) Laboratory, Rolla,MO,USA.Hiscurrentresearchinterestsincludenanometer-scaledevices, through-silicon via technology, signal integrity, power integrity, temperature integrity,EMC,andelectrostaticdischargein2.5-D/3-Dintegratedcircuitsystems.

Victor Khilkevich (Member, IEEE) received the Ph.D. degree in electrical engineering from Moscow Power Engineering Institute, Technical University, Moscow, Russia, in 2001.

He is currently an Assistant Professor with the Missouri University of Science and Technology, Rolla, MO, USA. His research interests include microwave imaging, automotive electromagnetic compatibility modeling, and high-frequency measurement techniques.

Bo Pu (Member, IEEE) received the B.S. degree in electrical engineering from the Harbin Institute of Technology, Harbin, China, in 2009, and the Ph.D. degree in electronic and electrical engineering from Sungkyunkwan University, Seoul, South Korea, in 2015.

In 2015, he joined Semiconductor R&D Division, Samsung Electronics, Hwaseong, South Korea, where he is currently a Staff Engineer. His research interests include the design methodology for chip-package-printed circuit board systems in the areas of signal integrity, power integrity, and electromagnetic compatibility. He recently focuses on the research of high-speed integrated circuits (ICs) system up to 112 Gbps, 2.5-D Si-interposer for high-bandwidth memory, and through silicon via for 3-D ICs. He holds ten patents about high-speed links and 2.5-D/3-D ICs.

Dr. Pu was a recipient of the Best Student Paper Award at the IEEE APEMC 2011 and a Young Scientists Award from the International Union of Radio Science in 2014. He was also a Session Chair in IEEE APEMC 2017 and a TPC member of the Joint IEEE EMCS and APEMC 2018. He is an Associate Editor for the *IEEE Access*.

Xiaoning Ye received the bachelor's and master's degrees in electronics engineering from Tsinghua University, Beijing, China, in 1995 and 1997, respectively, and the Ph.D. degree in electrical engineering from the University of Missouri–Rolla (currently the Missouri University of Science and Technology), Rolla, MA, USA, in 2000.

He is currently a Principal Engineer with Intel Corporation, Hillsboro, OR, USA, responsible for signal integrity of high-speed interconnects in server systems. He has authored or coauthored more than 100 IEEE and other technical papers, and holds 15 patents and a few more patent applications.

Dr. Ye was a recipient of the Technical Achievement Award from IEEE Electromagnetic Compatibility (EMC) Society in 2015. He is currently a member of the Board of Directors of EMC Society and served as a Chair of the Technical Advisory Committee for IEEE EMC Society in 2018–2020. He also chaired IEEE 370 standard development workgroup and IPC D24D task force.

QianGao received the Ph.D. degree in electrical engineering from Oregon State University, Corvallis, OR, USA, in 2018.

She is currently a Hardware Engineer with Cisco System, Inc., San Jose, CA, USA. Her research interests include signal integrity, silicon photonics, and optical transceivers.

Xiao-Ding Cai (Member, IEEE) received the Ph.D. degree in electrical engineering from the University of Ottawa, Ottawa, ON, Canada, in 1995.

He has been a High-Speed Signal Integrity Engineer assuming different responsibilities for Nortel Networks, Ottawa, ON, Canada; Sun Microsystems, Menlo Park, CA, USA; Juniper Networks, Sunnyvale, CA, USA; Rambus, San Jose, CA, USA; and Cisco System, Inc., San Jose, CA, USA.

Bidyut Sen received the Ph.D. degree in physics from the State University of New York, Stony Brook, NY, USA, in 1986.

He is a Principal Engineer with the Unified Compute Server Group, Cisco Systems, Inc., San Jose, CA, USA. He has many years of experience in the computer industry and has worked in several companies, including Sun

Microsystems, Fujitsu, and LSI Logic. He has several publications, presentations, and patents.

Jun Fan (Fellow, IEEE) received the B.S. and M.S. degrees in electronic engineering from Tsinghua University, Beijing, China, in 1994 and 1997, respectively, and the Ph.D. degree in electrical engineering from the University of Missouri-Rolla, Rolla, MA, USA, in 2000.

From 2000 to 2007, he was a Consultant Engineer with NCR Corporation, San Diego, CA, USA. In July 2007, he joined the Missouri University of Science and Technology (formerly University of Missouri-Rolla), where heis currently a CynthiaTangMissouriDistinguishedProfessorofcomputerengineeringandthe Director of the Electromagnetic Compatibility (EMC) Laboratory. His research interestsincludesignalintegrityandelectromagneticinterference(EMI)designs in high-speed digital systems, dc power-bus modeling, intrasystem EMI and RF interference, printed circuit board noise reduction, differential signaling, and cable/connector designs.

Dr. Fan was a recipient of the IEEE EMC Society Technical Achievement Award in August 2009. He serves as the Director of the National Science Foundation Industry/University Cooperative Research Center for EMC and a Senior Investigator of Missouri S&T Material Research Center. In the IEEE EMC Society, he served as the Chair of the TC-9 Computational Electromagnetics Committee from 2006 to 2008, the Chair of the Technical Advisory Committee from 2014 to 2016, and a Distinguished Lecturer in 2007 and 2008. He is currently an Associate Editor for the IEEE TRANSACTIONS ON ELECTROMAGNETIC COMPATIBILITY and IEEE EMC Magazine.